

Mechanism of Ti/Al/Ni/Au ohmic contacts to AlGaN/GaN heterostructures via laser annealing

Mingchen Hou(侯明辰), Gang Xie(谢刚), Kuang Sheng(盛况)

Citation: Chin. Phys. B . 2019, 28(3): 037302. **doi:** 10.1088/1674-1056/28/3/037302
Journal homepage: http://cpb.iphy.ac.cn; http://iopscience.iop.org/cpb

What follows is a list of articles you may be interested in

Effect of SiN: H_x passivation layer on the reverse gate leakage current in GaN HEMTs

Sheng Zhang(张昇), Ke Wei(魏珂), Yang Xiao(肖洋), Xiao-Hua Ma(马晓华), Yi-Chuan Zhang(张一川), Guo-Guo Liu(刘果果), Tian-Min Lei(雷天民), Ying-Kui Zheng(郑英奎), Sen Huang(黄森), Ning Wang(汪宁), Muhammad Asif, Xin-Yu Liu(刘新宇)

Chin. Phys. B . 2018, 27(9): 097309. **doi:** 10.1088/1674-1056/27/9/097309

Characteristics and threshold voltage model of GaN-based FinFET with recessed gate

Chong Wang(王冲), Xin Wang(王鑫), Xue-Feng Zheng(郑雪峰), Yun Wang(王允), Yun-Long He(何云龙), Ye Tian(田野), Qing He(何晴), Ji Wu(吴忌), Wei Mao(毛维), Xiao-Hua Ma(马晓华), Jin-Cheng Zhang(张进成), Yue Hao(郝跃)

Chin. Phys. B . 2018, 27(9): 097308. **doi:** 10.1088/1674-1056/27/9/097308

Schottky forward current transport mechanisms in AlGaN/GaN HEMTs over a wide temperature range

Wu Mei, Zheng Da-Yong, Wang Yuan, Chen Wei-Wei, Zhang Kai, Ma Xiao-Hua, Zhang Jin-Cheng, Hao Yue

Chin. Phys. B . 2014, 23(9): 097307. **doi:** 10.1088/1674-1056/23/9/097307

Effect of annealing on performance of PEDOT：PSS/n-GaN Schottky solar cells

Feng Qian, Du Kai, Li Yu-Kun, Shi Peng, Feng Qing

Chin. Phys. B . 2014, 23(7): 077303. **doi:** 10.1088/1674-1056/23/7/077303

A study of GaN MOSFETs with atomic-layer-deposited Al_2O_3 as the gate dielectric

Feng Qian, Xing Tao, Wang Qiang, Feng Qing, Li Qian, Bi Zhi-Wei, Zhang Jin-Cheng, Hao Yue

Chin. Phys. B . 2012, 21(1): 017304. **doi:** 10.1088/1674-1056/21/1/017304

Mechanism of Ti/Al/Ni/Au ohmic contacts to AlGaN/GaN heterostructures via laser annealing*

Mingchen Hou(侯明辰), Gang Xie(谢刚)†, and Kuang Sheng(盛况)

College of Electrical Engineering, Zhejiang University, Hangzhou 310027, *China*

(Received 20 November 2018; revised manuscript received 15 January 2019; published online 22 February 2019)

The physical mechanisms of Ti/Al/Ni/Au ohmic contacts to AlGaN/GaN heterostructures by laser annealing and rapid thermal annealing are systematically investigated. The microstructures indicate that a better surface morphology and an intact contact interface are formed after laser annealing. None of the TiN alloy spikes are formed at the interface of the laser annealing sample. The experimental results show that the current transport mechanism through the ohmic contact after laser annealing is different from the conventional spike mechanism, and it is dominated by thermionic field emission.

Keywords: gallium nitride, ohmic contacts, laser annealing, current transport mechanism

PACS: 73.61.Ey, 81.40.Rs, 68.37.Lp, 68.37.Ps **DOI:** 10.1088/1674-1056/28/3/037302

1. Introduction

GaN high electron mobility transistors (HEMTs) are promising devices for high-power and high-frequency applications.[1] Conventional AlGaN/GaN HEMTs are typically fabricated with Ti/Al/X/Au (X = Ni, Pt, Ti, Mo, etc.) ohmic contacts followed by a rapid thermal annealing (RTA) at above 800 °C.[2–9] The current transport mechanisms through the ohmic contact have been widely investigated.[10–15] The TiN protrusions are formed in correspondence with threading dislocations during the annealing process. A direct contact between metal and two-dimensional electron gas (2DEG) is established for the current flow. However, the TiN protrusions will cause undesired local electric field peaks and induce leakage current.[16–18] The large leakage current is undesired for the high-power applications. In addition, the conventional RTA process is responsible for rough morphology and metal boundary.[19] It will cause issues to the scaling down of the devices and will limit the high frequency performance.[20] In this case, it is highly desirable to develop high quality ohmic contacts for AlGaN/GaN HEMTs to enhance the performance and the reliability of the devices.

Laser annealing (LA) is widely used in device fabrication due to its high laser energy density and high annealing selectivity. The activation can be applied in a micron-scale area or a thin wafer instead of the whole wafer. Therefore, it significantly limits the induced thermal budget to the rest of a wafer. In the past few years, LA is used in the GaN-on-Si ohmic contact process.[21,22] However, it is more suitable for the GaN-on-SiC ohmic contact process. Because the energy band gaps of $Al_{0.25}Ga_{0.75}N$ barrier layer (3.9 eV), GaN channel layer (3.4 eV), and SiC substrate (3.25 eV) are all larger than the photon energy of the laser with a wavelength of 532 nm (2.33 eV), the wafer will not absorb the laser energy. Thus, it can avoid the thermal decomposition of GaN in the active region. Meanwhile, for the nitride-first technique, the stability of the electrical characteristics of the epitaxial materials and the stress in passivation layer can be improved. The ohmic contact formation process for AlGaN/GaN HEMTs based on pulsed laser annealing is reported in our previous work.[23] But a systematic investigation of the microstructure and physical mechanism of laser annealed ohmic contacts to AlGaN/GaN heterostructure is lacking. In this work, electrical measurements and a range of physical analysis tools including atomic force microscopy (AFM), focused ion beam (FIB), transmission electron microscopy (TEM), and energy dispersive x-ray spectroscopy (EDS) are used to investigate the morphology and composition of the ohmic contacts. The electrical and the structural results are coincident, which indicates that the current transport mechanism after laser annealing is different from the conventional spike mechanism.

2. Device fabrication

Both the LA samples and the conventional RTA samples are fabricated on AlGaN/GaN heterostructure grown on SiC substrate by NTT Corporation. The epitaxial structure consists of a 2 nm GaN cap layer, a 20 nm $Al_{0.25}Ga_{0.75}N$ barrier layer, a 200 nm unintentionally doped (UID) GaN channel layer, and a 1.8 μm carbon-doped GaN buffer layer. The AlGaN/GaN heterostructure features a 2DEG sheet resistance of 463.2 Ω/square and an electron mobility of 1360 $cm^2 \cdot V^{-1} \cdot s^{-1}$. The mesa isolation is done by using dry etching with Cl_2/BCl_3 mixture gas. The ohmic contacts are

*Projects supported by the National Natural Science Foundation of China (Grant Nos. 51577169 and 51777187) and the National Key Research and Development Program of China (Grant No. 2017YFB0402804).

†Corresponding author. E-mail: xielyz@zju.edu.cn

© 2019 Chinese Physical Society and IOP Publishing Ltd

formed with Ti/Al/Ni/Au by electron beam evaporation and then followed by LA. A laser with a wavelength of 532 nm, a pulse duration of 20 ns, a pulse frequency of 100 kHz, and an energy density of up to 3.22 J/cm^2 is used. The spot size is 5 mm × 5 μm and the scan speed is 40 mm/s. The reference sample is annealed by RTA at 840 °C–880 °C for 30 s in N_2 ambient.

3. Results and discussion

The *I*–*V* characteristics of the LA sample with various distance of transmission line measurement (TLM) patterns are illustrated in Fig. 1. The linear characteristics indicate that good ohmic contacts are formed between metal and semiconductor.

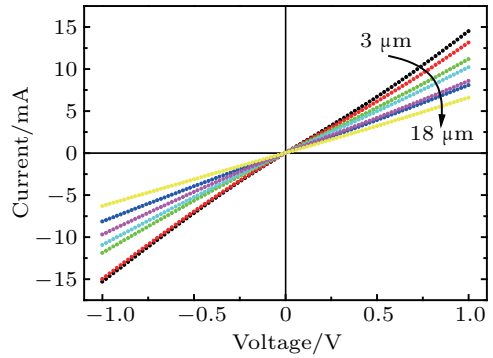


Fig. 1. *I*–*V* characteristics of TLM structures after LA at a laser energy density of 2.99 J/cm^2.

The contact resistances R_C are extracted from TLM. R_C with various annealing temperatures and various laser energy densities is shown in Fig. 2. As a result, a gradual reduction of contact resistance is observed as the annealing temperature and the laser energy density increase. The best results are obtained at the annealing temperature of 860 °C and the laser energy density of 2.99 J/cm^2. A further increase of the annealing temperature and the laser energy density results in a small increase of contact resistance because of the intermixing of the metal layers.[24,25]

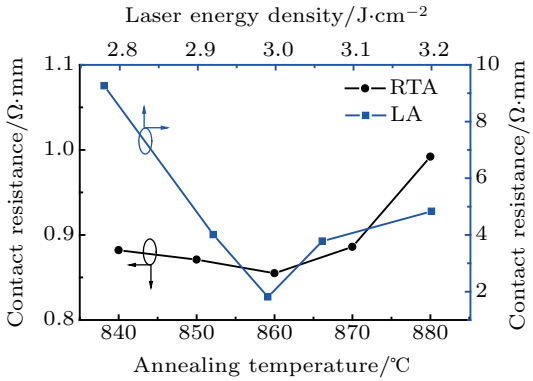


Fig. 2. The contact resistance as a function of the annealing temperature for the RTA sample and the laser energy density for the LA sample, respectively.

The AFM and optical microscope images of the surface morphology for the ohmic structure without annealing, after RTA at 860 °C for 30 s in N_2 ambient, and after LA at a laser energy density of 2.99 J/cm^2 are shown in Figs. 3(a), 3(b), and 3(c), respectively. The surface morphology of the RTA sample becomes rougher during the annealing, because the Al metal of the stacked Ti/Al/Ni/Au metal melts at above 800 °C and the large alloy grains are formed. In contrast, the surface morphology of the LA sample is smooth during the annealing as a result of the extremely short annealing time of LA.

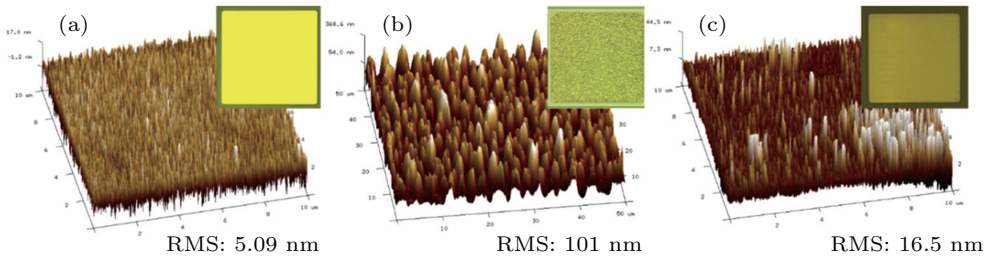


Fig. 3. The AFM and optical microscope images of the surface morphology for the ohmic structure (a) without annealing, (b) after RTA at 860 °C for 30 s in N_2 ambient, and (c) after LA at a laser energy density of 2.99 J/cm^2. RMS in the figure stands for root mean square.

In order to obtain a quantitative description of the transport mechanisms through the ohmic contact, the temperature dependence of the specific contact resistance ρ_C is studied for the RTA sample and the LA sample. The ρ_C values are monitored in a temperature range between 25 °C and 200 °C. As we can see in Fig. 4, for the samples with RTA, an increase of ρ_C with the increase of the measurement temperature is observed. For this annealing condition, the experimental data are fitted by the function $\rho_C \sim T^{\alpha}$, with $\alpha = 1.38$. This dependence suggests a "metal-like" behavior which has already been observed by other authors.[10,26] The resistance varies following a similar power law with $1 < \alpha < 5$ in metallic systems.

On the contrary, a different behavior is observed after LA, where ρ_C decreases as the measurement temperature increases. In this case, the behavior could be explained in terms of thermionic field emission (TFE) model. Accordingly, ρ_C is expressed as[27]

$$\rho_C = C_1 \frac{k}{qA^*T} e^{q\phi_B/E_0}, \tag{1}$$

where E_0 in Eq. (1) is related to E_{00} by

$$E_0 = E_{00} \coth\left(E_{00}/kT\right). \tag{2}$$

The characteristic energy E_{00} is defined by

$$E_{00} = \frac{qh}{4\pi}\sqrt{\frac{N_D}{m^*\varepsilon}}, \tag{3}$$

where m^* is the tunneling effective mass, ϕ_B is the barrier height, N_D is the carrier concentration, and C_1 is a function of N_D, T, and ϕ_B. The values of $\phi_B = 0.58$ eV and $N_D = 0.82 \times 10^{19}$ cm^{-3} are extracted, which are similar to the experimental values obtained by other authors.[10,28,29]

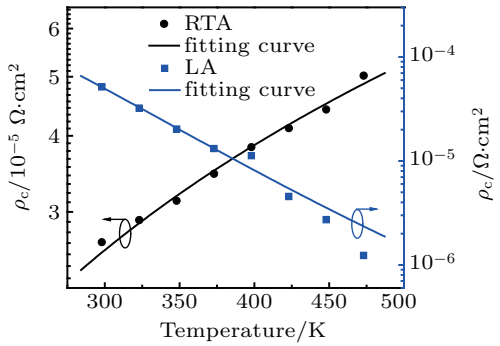


Fig. 4. The specific contact resistance as a function of the measured temperature for the RTA sample and LA sample, respectively.

In order to explain the experimental data of the electrical measurements, a structural analysis of both annealed metal/AlGaN/GaN stacks is carried out by means of TEM. The cross-sectional TEM micrographs of the samples with RTA and LA are shown in Figs. 5(a)–5(d). The surface of the metal layers is marked by the red dashed line in Figs. 5(a) and 5(b). The material outside the red dashed line is Pt. It is deposited during the FIB fabrication. As can be seen, a rough morphology of the metal layers is observed in the RTA sample in Fig. 5(a). A large quantity of alloy aggregations are formed during the RTA process. On the contrary, a smoother surface of the metal layers is observed in the LA sample in Fig. 5(b). The dividing lines of the metal layers are clear.

Moreover, in the RTA sample, obvious metal spikes are observed at the contact interface, probably along dislocations in Fig. 5(c). The metal spikes penetrate the AlGaN layer and direct contact the 2DEG. They create preferential paths for the current flow and make the current transport more efficient. Thus, the current transport mechanism of RTA sample is dominated by spike mechanism. On the contrary, a distinct ohmic contact interface can be observed in the LA sample in Fig. 5(d). None of the metal spikes are observed at the interface between the Ti layer and the AlGaN layer. In this case, the current transport mechanism should be different from the conventional spike mechanism. Electrons transport through the AlGaN barrier by thermionic emission due to the lack of spike. Meanwhile, Ti absorbs nitrogen from the AlGaN layer during the interface reaction which results in the creation of nitrogen vacancies within the AlGaN layer. These vacancies in turn play the role of n-type dopants. As a result, an additional path is formed for electron transport via trap assisted tunneling in AlGaN/GaN heterostructures.[30] Therefore, the current transport mechanism of LA sample is dominated by TFE. According to our description, a schematic of the energy band diagram is shown in Fig. 6.

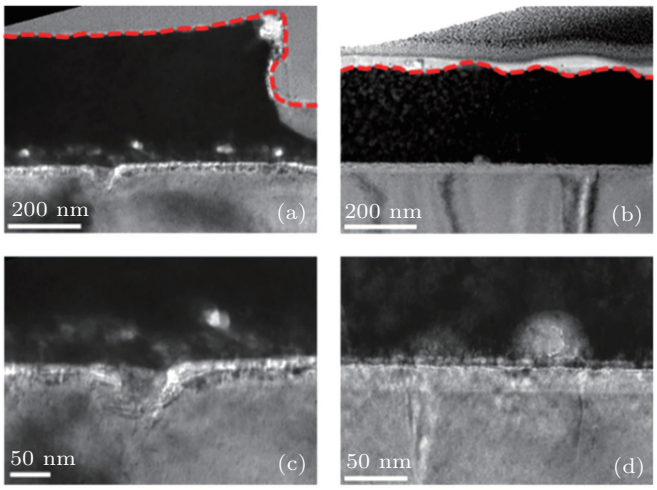


Fig. 5. The cross-sectional TEM micrographs of ohmic contacts to AlGaN/GaN heterostructures annealed by (a) RTA and (b) LA. Higher magnification is acquired in the proximity of the interface for (c) RTA sample and (d) LA sample.

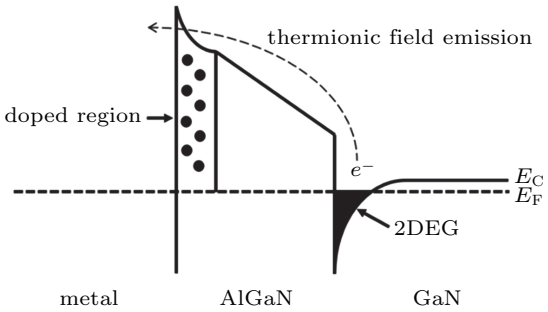


Fig. 6. Schematic of the energy band diagram for the contacts annealed by LA.

EDS is carried out in order to investigate the composition of different layers. Figure 7 shows the EDS mappings of the metal layers of RTA and LA samples. In the RTA sample, Al–Au alloy aggregation and Al–Ni alloy aggregation are formed in the metal stack layers. They are responsible for a rough morphology. However, in the LA sample, it is clear that none of the alloy aggregations are observed in the metal stack layers. An intact Al–Ni–Au alloy layer is formed during laser annealing. Thus, the surface morphology is improved. In addition, a Ti–Al alloy layer is formed between the Al–Ni–Au alloy layer and the AlGaN layer. It is conducive to reduce the contact resistance.

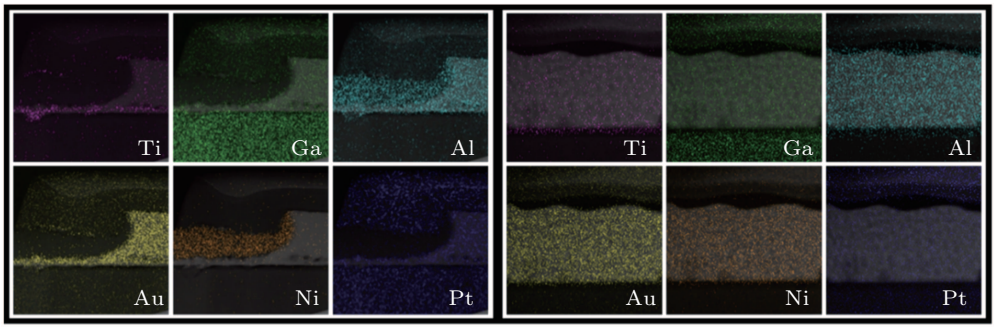


Fig. 7. The compound images of the scanning transmission electron microscope (STEM) and the EDS mappings for the metal layers of the (a) RTA sample and the (b) LA sample.

Figure 8 shows the EDS mappings of the interface of the contact in the RTA and the LA samples. In the RTA sample, TiN spike is clearly visible in the AlGaN/GaN heterostructure after the interfacial reactions. The EDS mappings show that the TiN spike is surrounded by a thin AlN layer. At the same time, Au is diffused to the interface of the contact through Ni barrier layer. On the contrary, in the LA sample, the boundaries of the Al–Ni–Au alloy layer, the Ti–Al alloy layer, the AlGaN layer, and the GaN layer are intact. None of the TiN spikes are observed at the contact interface. It is conducive to reduce the leakage current and improve the reliability of the devices.

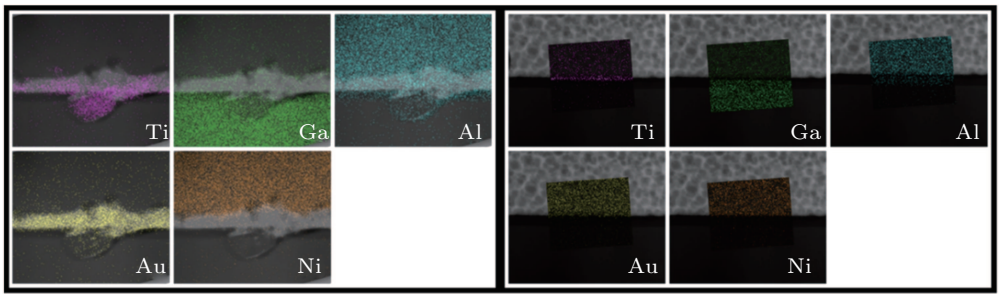


Fig. 8. The compound images of the STEM and the EDS mappings for the contact interface of the (a) RTA sample and the (b) LA sample.

4. Conclusion

In summary, for the RTA and the LA samples, the correlation between the electrical and the structural properties of Ti/Al/Ni/Au ohmic contacts to AlGaN/GaN heterostructures is reported. The physical mechanism is systematically investigated by a range of physical analysis tools, such as AFM, FIB, TEM, and EDS. The current transport mechanism through the ohmic contact after laser annealing is dominated by thermionic field emission. These results indicate that laser annealing is a method to improve the surface morphology and the quality of the contact interface.

References

[1] Umesh K M, Shen L K, Kazior T E and Wu Y F 2008 *Proc. IEEE* **96** 287

[2] Lim J H, Kim J J and Yang J W 2015 *Microelectron. Reliab.* **55** 2565

[3] Fay M W, Han Y, Brown P D, Harrison I, Hilton K P, Munday A, Wallis D, Balmer R S, Uren M J and Martin T 2008 *J. Appl. Phys.* **103** 074501

[4] Chen J, Ivey D G, Bardwell J, Liu Y, Tang H and Webb J B 2002 *J. Vac. Sci. & Technol. A* **20** 1004

[5] Wang L, Mohammed F M and Adesida I 2007 *J. Appl. Phys.* **101** 013702

[6] Zhang T, Pu T F, Xie T, Li L A, Bu Y Y, Wang X and Ao J P 2018 *Chin. Phys. B* **27** 078503

[7] Liu Y, Lin Z J, Lv Y J, Cui P, Fu C, Han R L, Huo Y and Yang M 2017 *Chin. Phys. B* **26** 097104

[8] Cui P, Lin Z J, Fu C, Liu Y and Lv Y J 2017 *Chin. Phys. B* **26** 127102

[9] Yang L, Zhou X W, Ma X H, Lv L, Cao Y R, Zhang J C and Hao Y 2017 *Chin. Phys. B* **26** 017304

[10] Iucolano F, Greco G and Roccaforte F 2013 *Appl. Phys. Lett.* **103** 201604

[11] Zhang J H, Huang S, Bao Q L, Wang X H, Wei K, Zheng Y K, Li Y K, Zhao C, Liu X, Zhou Q, Chen W J and Zhang B 2015 *Appl. Phys. Lett.* **107** 262109

[12] Greco G, Iucolano F and Roccaforte F 2016 *Appl. Surf. Sci.* **383** 324

[13] Whiting P G, Rudawski N G, Holzworth M R, Pearton S J, Jones K S, Liu L, Kang T S and Ren F 2017 *Microelectron. Reliab.* **70** 41

[14] Graff A, Simon-Najasek M, Altmann F, Kuzmik J, Gregušová D, Haščík Š, Jung H, Baur T, Grünenpütt J and Blanck H 2017 *Microelectron. Reliab.* **76-77** 338

[15] Wang L, Zhang J Q, Li L A, Maeda Y T and Ao J P 2017 *Chin. Phys. B* **26** 037201

[16] Lian Y W, Lin Y S, Lu H C, Huang Y C and Hsu S S H 2012 *IEEE Electron Device Lett.* **33** 973

[17] Tang C, Xie G and Sheng K 2015 *Microelectron. Reliab.* **55** 347

[18] Pooth A, Bergsten J, Rorsman N, Hirshy H, Perks R, Tasker P, Martin T, Webster R F, Cherns D, Uren M J and Kuball M 2017 *Microelectron. Reliab.* **68** 2

[19] Gong R M, Wang J Y, Liu S H, Dong Z H, Yu M, Wen C P, Cai Y and Zhang B S 2010 *Appl. Phys. Lett.* **97** 062115
[20] Tsou C W, Kang H C, Lian Y W and Hsu S S H 2016 *IEEE Trans. Electron. Devices* **63** 4218
[21] Tzou A J, Hsieh D H, Chen S H, Li Z Y, Chang C Y and Kuo H C 2016 *Semicond. Sci. Technol.* **31** 055003
[22] Ferreyra R A, Suzuki A, Kazumoto T and Ueda D 2017 *IEEE Electron Device Lett.* **38** 1079
[23] Hou M C, Xie G and Sheng K 2018 *IEEE Electron Device Lett.* **39** 1137
[24] Schmid A, Schroeter C, Otto R, Schuster M, Klemm V, Rafaja D and Heitmann J 2015 *Appl. Phys. Lett.* **106** 053509
[25] Piazza M, Dua C, Oualli M, Morvan E, Carisetti D and Wyczisk F 2009 *Microelectron. Reliab.* **49** 1222
[26] Greco G, Giannazzo F, Iucolano F, Nigro R L and Roccaforte F 2013 *J. Appl. Phys.* **114** 083717
[27] Schroder D K 2006 *Semiconductor Material and Device Characterization* (3rd edn.) (Hoboken: John Wiley & Sons) p. 133
[28] Liu Z H, Arulkumaran S and Ng G I 2009 *Appl. Phys. Lett.* **94** 142105
[29] Iucolano F, Roccaforte F, Alberti A, Bongiorno C, Franco S D and Raineri V 2006 *J. Appl. Phys.* **100** 123706
[30] Upadhyay P, Meer M, Takhar K, Khachariya D, Kumar S A, Banerjee D, Ganguly S, Laha A and Saha D 2015 *Phys. Status Solidi B* **252** 989